



HAL
open science

Dynamic feedback linearization and singular perturbation for a stabilizing controller for dc/dc boost converters: theory and experimental validation

Qihao Guo, Miguel Jimenez Carrizosa, Alessio Iovine, Amir Arzande

► To cite this version:

Qihao Guo, Miguel Jimenez Carrizosa, Alessio Iovine, Amir Arzande. Dynamic feedback linearization and singular perturbation for a stabilizing controller for dc/dc boost converters: theory and experimental validation. IEEE Transactions on Industrial Electronics, 2023, pp.1 -10. 10.1109/TIE.2023.3312425 . hal-04198531

HAL Id: hal-04198531

<https://centralesupelec.hal.science/hal-04198531>

Submitted on 7 Sep 2023

HAL is a multi-disciplinary open access archive for the deposit and dissemination of scientific research documents, whether they are published or not. The documents may come from teaching and research institutions in France or abroad, or from public or private research centers.

L'archive ouverte pluridisciplinaire **HAL**, est destinée au dépôt et à la diffusion de documents scientifiques de niveau recherche, publiés ou non, émanant des établissements d'enseignement et de recherche français ou étrangers, des laboratoires publics ou privés.

Dynamic feedback linearization and singular perturbation for a stabilizing controller for dc/dc boost converters: theory and experimental validation

Qihao Guo, Miguel Jiménez Carrizosa, Alessio Iovine, *Member, IEEE*, and Amir Arzandé

Abstract—The current massive integration of constant power loads (CPLs) requires better dynamic performance in Direct Current (DC) microgrids. This imposes the needs for more advanced controllers for DC/DC converters, and especially for boost ones because of their non-minimum phase property. The current paper contributes to this research line and proposes an advanced nonlinear (NL) control strategy for the output voltage stabilization of boost converters using singular perturbation and dynamic feedback linearization strategies. The proposed techniques manages to impose a desired stable dynamics for the variable with the non-minimum phase characteristics, thus avoiding the problem of possible selection of unstable equilibria. At first, a theoretical proof of the stability of the close loop system with the proposed controller is provided. Then, an experimental validation composed by four case studies is performed. The results show good adaptability to a wide range of operating conditions and better performance regarding voltage tracking and load disturbances rejection of the proposed NL method with respect to classical control techniques.

Index Terms—Boost converter, Nonlinear control, time-scale separation, Lyapunov theory, constant power load

I. INTRODUCTION

With the worldwide rise of energy needs, power electronics plays a crucial role in technological development because of the importance of power converters in modern power systems. Indeed, power converters are used in a wide range of applications, for example, renewable sources, battery banks, the transmission of electrical energy in direct current (HVDC), smart grids, FACTS, active filters, etc [1].

On the other hand, Direct Current (DC) Microgrids have reached a high degree of development in the last decade [2]. Their main purpose is on exploiting energy management from renewable sources on a small and local scale. DC grids offer several advantages over AC ones, such as the absence of reactive power or skin effect in the cables, and an easier integration of renewable energies. Furthermore, since many modern loads, battery systems or photovoltaic (PV) panels are naturally in DC, DC Microgrids seem a good candidate to favour their integration.

Q. Guo and A. Arzandé is with the Group of Electrical Engineering of Paris (GeePs), CNRS, CentraleSupélec, Paris-Saclay University and Sorbonne University, 11, rue Joliot Curie Plateau de Moulon 91190 Gif sur Yvette, France. E-mail: {qihao.guo,amir.arzande}@centralesupelec.fr.

M. Jiménez Carrizosa is with the Centro de Electrónica Industrial, Universidad Politécnica de Madrid, 28006 Madrid, Spain. E-mail: miguel.jimenezcarrizosa@upm.es.

A. Iovine is with the Laboratory of Signal and Systems (L2S), Centre National de la Recherche Scientifique (CNRS), CentraleSupélec, Paris-Saclay University, 3, rue Joliot-Curie, 91192 Gif-sur-Yvette, France. E-mail: alessio.iovine@centralesupelec.fr.

This project has received funding from the Agence Nationale de la Recherche (ANR) via grant ESTHER ANR-22-CE05-0016.

As the DC bus voltage is usually higher compared to the terminal voltage of the energy sources, in many applications it is necessary to increase the voltage in order to connect them to the DC Microgrid, even when the voltage of the source is variable (e.g., in PV panels). Therefore, the use of DC/DC step-up boost converters is very popular [1]. Examples of their utilisation are battery-powered devices, since they require a higher voltage than the battery can provide in order to operate properly, or solar power systems, where the output voltage of the solar panels can vary depending on the amount of sunlight available and there is the need to maintain a constant output voltage from the solar panels, regardless of the input voltage and load variations.

Traditionally, linear control techniques were used in power converters, which have some limitations [3], [4], [5], [6], such as poor performance under nonlinear and dynamic operating conditions, and difficulty in handling the complex nonlinear dynamics of these systems. This is where advanced control techniques come in, since they are designed to overcome the limitations of traditional linear control methods by taking into account the nonlinear dynamics of power converters and offer several advantages, including improved performance and stability, robustness to external disturbances or uncertainties and improved performance under nonlinear and dynamic operating conditions [7]. These techniques include methods such as feedback linearization [8], [9], sliding mode control [10], [11], optimal approaches [12], [13], [14], [15], singular perturbation and multi-time scale theory [16], [17], hybrid systems approaches [4], [18], current limitations [19], etc. Additionally, the use of advanced nonlinear control techniques can lead to significant energy savings, e.g., by reducing the high rate of switching [18]. Therefore, investing in the development and implementation of these techniques is crucial for the future of power systems and the efficient use of energy resources.

As mentioned, one of the typical control objectives for boost converters is to regulate the output voltage given a (constant or time-varying) reference signal [20]. The dynamics of boost converter falls under the class of nonlinear systems, and more specifically of the one of bilinear ones. It is well known that the kind of systems describing the boost converters are complex to control because of their controllability properties [20], [4]. Indeed, when applying the classical feedback linearization nonlinear control technique, it produces local stability results with respect to a zero dynamic that needs to be ensured to be stable [8], [9]. This is due to the structural property that the relative degree of the system, i.e., one, is less than the number of variables in the system, i.e., two [21], [22], [23], which results in an undesired non-minimum

phase behavior for the variable that is not directly controlled [24]. Similarly, the intrinsic non-minimum phase behaviour also affects the possibility of considering different nonlinear control techniques, for example, backstepping, which cannot be directly used, or sliding mode, since the computation of performing sliding surfaces is hard and has to take into account to define a locally stable zero dynamics [20], [10], [11]. Moreover, the non-minimum phase problem makes it difficult to obtain high bandwidth controllers even when the classical PI technique is applied [12]. Therefore, the control problem is severely affected by the necessity to investigate the stability region for the zero dynamics (for more details about the stable and unstable equilibrium points for DC/DC boost converters, the interested reader is referred to [25]).

In the present paper, we focus on the possibility of imposing the desired stable dynamics for the not directly controlled variable presenting the non-minimum phase characteristics, i.e., the voltage of the output capacitor. To ensure stable performance via Lyapunov analysis, the suggested controller uses different nonlinear control techniques in a backstepping-like approach, namely singular perturbation theory [26] and dynamic feedback linearization [27]. The developed controller considers singular perturbation theory [26] for the needed time-scale separation and falls in the research lines of [16], [17], [28]. The novelty in the suggested control design is to consider both singular perturbation and dynamic feedback linearization thus to embed the stability of the non-minimum phase dynamics while developing the controller. This ensures the stability of the non-minimum phase dynamics while the controller is developed, which is a stronger result than only having stability verification a posteriori, as for example in [16]. Indeed, it opens to the possibility to better select the current reference with respect to the dynamics of the non-minimum phase dynamics, thus resulting in a more effective behaviour of the closed loop system and the possibility to modify the stability region with respect to it [29]. Rather than just analysis of the non-minimum phase dynamics with respect to the equilibrium point, the suggested controller manages to impose the desired stable dynamics, thus avoiding the problem of selection of unstable equilibria (see [25]). We leverage previous theoretical results [30], [31] dedicated to microgrid applications while providing a general description of the controller, and perform experimental tests with respect to a resistive load and a Constant Power Load (CPL). Indeed, CPLs, which have significantly proliferated in recent times, exhibit negative incremental impedance and cause serious instability issues in boost converters [32], [33], [34]. Therefore, they are the perfect test for the suggested controller.

The paper is organized as follows. Section II introduces the modelling of the DC/DC Boost converter. In Section III, the proposed nonlinear controller is introduced, and stability results are discussed. In Section IV, the experimental results are shown. Finally, in Section V, the main conclusions are exposed.

II. MODELLING

Fig. 1 shows the circuit layout of the considered DC/DC boost converter. If the converter is operating in continuous conduction mode (CCM), there are two linear dynamics according to the positions of the switch S (ON or OFF). When the switch is ON ($S = 1$), the energy from the input voltage source is transferred to the inductance L and therefore the current in the inductance x_L increases. When the switch is OFF ($S = 0$) and $x_L > 0$, the energy stored in the inductance is transferred to the load, leading to the decrease of x_L . The diode D does not allow the current to flow back. The voltage in the capacitor C , i.e., $x_C > 0$, clearly varies with respect to x_L and the load.

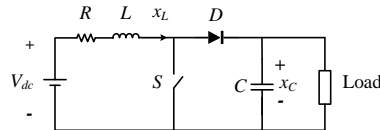


Fig. 1. The electrical scheme of the boost converter

By averaging the inductance current and capacitor voltage over a switching period, a boost converter is usually described by an averaged nonlinear model. The dynamics are described by a nonlinear dynamical system in the form of:

$$\begin{cases} \dot{x}_L = -\frac{R}{L}x_L + \frac{1}{L}V_{dc} - \frac{d}{L}x_C \\ \dot{x}_C = \frac{d}{C}x_L - \frac{1}{C}f(x_C) \end{cases} \quad (1)$$

where the state variables are x_L and x_C ; the control variable is the duty cycle d , and $f(x_C) = \frac{x_C}{R_{load}}$ in case of a resistive load, with R_{load} being the load resistance, or $f(x_C) = \frac{P}{x_C}$ in case of CPL, with P being the power demanded by the load. The parameters L , R , and C are the values of the inductance, its internal resistance, and the capacitor, respectively.

In the rest of the paper, the targeted control objective for the dynamics in (1) is to regulate the output voltage given a (constant or time-varying) reference signal [20].

III. NONLINEAR CONTROLLER

As already mentioned, the nonlinear dynamics of boost converters make them difficult to control. In the present paper, we suggest a methodology based on several nonlinear control techniques. We follow a backstepping-like approach, which allows us to separate the whole control target by taking care of the two dynamics separately. The following steps are:

- i) introduce a control input d such that the current variable x_L tracks a reference x_L^* , which can be a fixed known value or a function depending on time to be defined;
- ii) decouple the dynamics of x_L and x_C using singular perturbation theory;
- iii) define the time derivative of x_L^* as dynamic controller for stabilizing x_C using the dynamic feedback linearization;
- iv) find the reference value for \dot{x}_L^* to stabilise the system, and integrate it to obtain the reference x_L^* .

In the following, Section III-A describes the case where a fixed current reference is considered, thus performing i). Then, Section III-B considers the case where the voltage value is targeted via singular perturbation theory, thus performing ii). Then, Sections III-C and III-D describe how to compute the time derivative of the current reference and how to build the current reference with respect to it, respectively, then describing the points in iii) and iv). Therefore, the theoretical analysis ensuring stability is fulfilled. Finally, Section III-E describes the steps to implement the suggested controller and provides a scheme describing the different pieces the controller is composed by.

A. Current control via Lyapunov analysis

A controller based on Lyapunov theory that ensures asymptotic convergence of the current to the reference value x_L^* is developed in this section. To this goal, the candidate Lyapunov function in (2) is considered, which takes into account an integral term similarly to the well known Proportional-Integral (PI) technique, to obtain the desired controller.

$$W_L = \frac{1}{2}(x_L - x_L^*)^2 + \frac{1}{2}\beta \left(\int (x_L - x_L^*) \right)^2 \quad (2)$$

According to Lyapunov theory, the controller in (3) is obtained in a similar way as in [31] but adding in this case the integrator term:

$$d = \frac{1}{x_C} \left(\frac{V_{dc}}{L} - \frac{R}{L}x_L - \dot{x}_L^* + \beta \int (x_L - x_L^*) + \alpha(x_L - x_L^*) \right) \quad (3)$$

Indeed, by simple computations of the time derivative of (2), i.e., \dot{W}_L as

$$\begin{aligned} \dot{W}_L &= (x_L - x_L^*)(\dot{x}_L - \dot{x}_L^*) + \beta(x_L - x_L^*) \int (x_L - x_L^*) \\ &= (x_L - x_L^*) \left(-\frac{R}{L}x_L + \frac{1}{L}V_{dc} - \frac{1}{L}dx_C - \dot{x}_L^* \right) \\ &\quad + \beta(x_L - x_L^*) \left(\int (x_L - x_L^*) \right), \end{aligned} \quad (4)$$

it is possible to show that the controller in (3) ensures asymptotic stability of x_L with respect to x_L^* . In fact, \dot{W}_L is negative semi-definite:

$$\dot{W}_L = -\alpha(x_L - x_L^*)^2 \leq 0. \quad (5)$$

From (5), it results $\dot{W}_L(t) \leq \dot{W}_L(0)$, which implies that $x_L - x_L^*$ and $\int x_L - x_L^*$ are bounded, thanks to Lyapunov theorem. Consequently, by computing \ddot{W}_L , it can be shown that it is bounded as well, since composition of bounded functions. Therefore, \dot{W}_L is uniformly continuous over time. By applying Barbalat's lemma, it is then possible to establish asymptotic convergence, i.e., $\dot{W}_L \rightarrow 0$ as $t \rightarrow +\infty$.

In (3), the nature of the reference x_L^* is not defined. We remark that $\dot{x}_L^* = 0$ in case of fixed reference. For sake of generality, we consider this terms in (3). The controller in (3) is adopted for both the case of resistive load or CPL in (1); the difference with respect to the different characteristics of the situations will be exploited in Section III-B.

B. Time-scale separation of dynamics via singular perturbation theory

Here, we allow the controller in (3) to consider a time-varying reference for x_L^* , that can be defined with respect to a desired voltage value x_C^* . To this purpose, we first decouple the dynamics of x_L and x_C , as described in ii). Therefore, we rewrite the closed-loop equations according to singular perturbation form (see [31], [26]).

1) *Constant resistance load*: In case of resistive load in (1), it results:

$$\begin{cases} C\dot{x}_C = dx_L - \frac{1}{R_{load}}x_C \\ \frac{1}{\alpha}\dot{x}_L = -(x_L - x_L^*) - \frac{\beta}{\alpha} \int (x_L - x_L^*) \end{cases} \quad (6)$$

As described in [31], if the control gain α is large enough such that $\frac{1}{\alpha} \rightarrow 0$, we have $x_L = x_L^*$. Therefore, with this assumption we obtain the reduced model for \dot{x}_C as:

$$\dot{x}_C = \frac{1}{C} \frac{1}{x_C} \left(\frac{V_{dc}}{L} - \frac{R}{L}x_L^* \right) x_L^* - \frac{1}{C} \frac{1}{R_{load}}x_C \quad (7)$$

Let us define the error e_C of the voltage x_C with respect to the desired value x_C^* ,

$$e_C = x_C - x_C^* \quad (8)$$

and rewrite the error dynamics of \dot{e}_C as

$$\begin{aligned} \dot{e}_C &= \frac{V_{dc}}{CL} \frac{x_L^*}{e_C + x_C^*} - \frac{R}{CL} \frac{(x_L^*)^2}{e_C + x_C^*} - \frac{1}{C} \frac{1}{R_{load}}(e_C + x_C^*) \\ &= a_1 \frac{x_L^*}{e_C + x_C^*} - a_2 \frac{(x_L^*)^2}{e_C + x_C^*} - a_3(e_C + x_C^*), \end{aligned} \quad (9)$$

where

$$a_1 = \frac{V_{dc}}{CL}, \quad a_2 = \frac{R}{CL}, \quad a_3 = \frac{1}{C} \frac{1}{R_{load}}. \quad (10)$$

2) *Constant power load*: Similarly to the previous case, we rewrite the system according to singular perturbation theory:

$$\begin{cases} C\dot{x}_C = dx_L - \frac{P}{x_C} \\ \frac{1}{\alpha}\dot{x}_L = -(x_L - x_L^*) - \frac{\beta}{\alpha} \int (x_L - x_L^*) \end{cases} \quad (11)$$

Therefore, similarly to the case of constant resistance load, the reduced model for \dot{x}_C results:

$$\dot{x}_C = \frac{1}{C} \frac{1}{x_C} \left(\frac{V_{dc}}{L} - \frac{R}{L}x_L^* \right) x_L^* - \frac{1}{C} \frac{P}{x_C} \quad (12)$$

and the error dynamics e_C is

$$\dot{e}_C = \frac{a_1 x_L^* - a_4}{e_C + x_C^*} - a_2 \frac{(x_L^*)^2}{e_C + x_C^*}, \quad (13)$$

where $a_4 = \frac{P}{C}$.

C. Time derivative of the current reference as degree of freedom

Since the boost converters have not a single equilibrium point, we target to consider the stable one(s) by imposing a stable dynamics (see [25]). By using dynamic feedback linearization, we look for the reference x_L^* that stabilizes e_C . To do this, we extend the state and compute the time derivative of \dot{e}_C .

1) *Constant resistance load:* It results

$$\begin{aligned} \ddot{e}_C &= \left(\frac{a_2(x_L^*)^2 - a_1x_L^* - a_3}{(e_C + x_C^*)^2} \right) \dot{e}_C + \frac{a_1 - 2a_2x_L^*}{e_C + x_C^*} \dot{x}_L^* \\ &= L_e^2 + L_g \dot{x}_L^* \end{aligned} \quad (14)$$

2) *Constant power load:* It results

$$\begin{aligned} \ddot{e}_C &= \left(\frac{a_2(x_L^*)^2 - a_1x_L^* - a_4}{(e_C + x_C^*)^2} \right) \dot{e}_C + \frac{a_1 - 2a_2x_L^*}{e_C + x_C^*} \dot{x}_L^* \\ &= L_e^2 + L_g \dot{x}_L^* \end{aligned} \quad (15)$$

We remark that the notation L_e^2 and L_g refers to the classical Lie brackets [21] for feedback linearisation and dynamic feedback linearisation.

D. Current reference for linear closed loop system

It is now possible to use the degree of freedom in defining \dot{x}_L^* to stabilize the extended system. By considering the integral error term $\xi_1 = \int e_C$, the error term $\xi_2 = e_C$ and its time derivative $\xi_3 = \dot{e}_C$, it results

$$\begin{cases} \dot{\xi}_1 = \xi_2 \\ \dot{\xi}_2 = \xi_3 \\ \dot{\xi}_3 = L_e^2 + L_g \dot{x}_L^* \end{cases} \quad (16)$$

Therefore, by choosing

$$\dot{x}_L^* = \frac{1}{L_g} \left[-L_e^2 - K_1^\xi \xi_1 - K_2^\xi \xi_2 - K_3^\xi \xi_3 \right] d\tau \quad (17)$$

it clearly results that the closed loop system in (16) has stable eigenvalues for positive values of K_1^ξ , K_2^ξ and K_3^ξ , since the closed loop matrix A_ξ of the resulting linear system is in the canonical control form:

$$A_\xi = \begin{pmatrix} 0 & 1 & 0 \\ 0 & 0 & 1 \\ -K_1^\xi & -K_2^\xi & -K_3^\xi \end{pmatrix} \quad (18)$$

We remark that the system in (16) considers both a proportional and an integral action for the voltage control, as standard in power electronics. Therefore, classical techniques for tuning of control parameters can be applied. Finally, to obtain the desired x_L^* it suffices to integrate over time the reference in (17), i.e.,

$$x_L^* = \int_0^t \dot{x}_L^*(\tau) d\tau. \quad (19)$$

E. Control algorithm

The suggested control strategy is shown in Fig. 2. The steps to execute the proposed control strategy are:

- 1) given the voltage reference x_C^* , to implement the controller suggested in (3);
- 2) to tune the control gains α and β with respect to the desired dynamics for the current;
- 3) to compute the current reference x_L^* as in (19), where the time derivative \dot{x}_L^* in (17) is defined by the functions L_e^2 and L_g in (14) in case of resistive load or in (15) if CPL, respectively;

- 4) to tune the control gains K_1^ξ , K_2^ξ and K_3^ξ with respect to the desired dynamics for the voltage.

We remark that the choice of the control gains has to respect the hypothesis that α is large enough such that the reduced models in (7) and (12) make sense (see [28]). As shown in Fig. 2 and Table I, there is a difference between the gains for the fast loop and the slow one. Indeed, as it is also possible to notice from the equation defining d in (3), the current control part compensates the parameter L , and therefore the control parameters α and β in the fast loop can be chosen in the order of magnitude for imposing the eigenvalues for the closed loop system such that they are larger than the ones imposed naturally by $\frac{1}{L}$. Therefore, a rule for tuning them is to consider them as multiple values of $\frac{1}{L}$, e.g., α being five or ten times $\frac{1}{L}$. On the contrary, in the slow loop the gains K_1^ξ , K_2^ξ and K_3^ξ have to compensate the division by C (see the coefficients a_1 , a_2 , a_3 and a_4 in (10)) to maintain the same order of magnitude of $\frac{1}{C}$, and therefore a tuning rule for them is to consider the fact that they need to be divided by C and at the same time be multiple values of $\frac{1}{C}$.

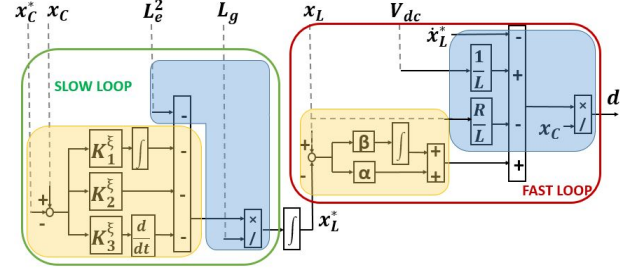


Fig. 2. The adopted control scheme producing the duty cycle d . The figure shows the fast current loop and the slow voltage one, which are based on time-scale separation. The feedback linearizing parts are depicted in dark blue, while the equivalent PI and PID are depicted in light yellow.

IV. EXPERIMENTAL RESULTS

This section describes the obtained experimental results when applying the suggested nonlinear (NL) controller for tracking a desired reference for the output voltage. Two different voltage strategies (variable reference voltage and constant reference with load variation) are carried out. In addition, for each of these strategies two different types of loads are used, i.e., resistive loads and CPL, thus resulting in a total of four experiments. For each of them, a fair comparison between the PI controller and the proposed nonlinear controller is carried out.

A. The experimental testbed

A picture of the experimental bench is shown in Fig. 3. The boost converter module is driven by ARCAL 2108 driver board supplied by ARCEL. A dSPACE MicroLabBox 1202 is used to implement the control strategies with a sampling time of $50\mu\text{s}$. A DELTA ELEKTRONIKA SM500-CP-90 controllable voltage source is used to emulate the DC input voltage. An EA-ELR 9250-70 controllable power electronic load is used

to represent the CPL, in addition to the available resistance load. The software ControlDesk from dSPACE is used for supervision. The detailed circuit and controller parameters are given in Table I.

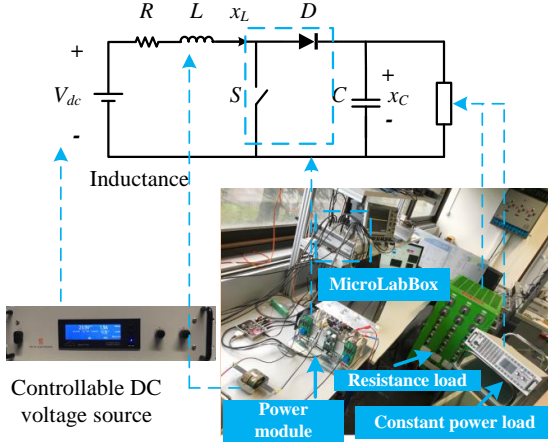


Fig. 3. Experimental setup

TABLE I
EXPERIMENTAL PARAMETERS

Experimental parameters		
Input resistance	R	0.003Ω
Input inductance	L	$175 \mu\text{H}$
Input voltage	V_{in}	24 V
Output capacitor	C	$2220 \mu\text{F}$
Output voltage	V_{out}	48 V
Switch frequency	f_s	20 kHz
PI control parameters		
Voltage loop proportional constant	K_p	0.3
Voltage loop integral constant	K_i	15
Current loop proportional constant	K_p	0.03
Current loop integral constant	K_i	56
Backstepping control parameters		
Error term (current)	α	1
Integral error term (current)	β	200
Integral error term (voltage)	K_1^ξ	15000
Error term (voltage)	K_2^ξ	400
Derivative error term (voltage)	K_3^ξ	1

B. Nonlinear and PI controller parameters tuning

Since it is one of the most popular control strategies for the boost converter, the linear controller-based average current-mode control is selected as reference method to compare the performance of the proposed NL control strategy. To produce a fair comparison between these two controllers, the 95% settling time for output voltage control is used as a criterion. In this study, the 95% settling time is set to be around 100 ms without loss of generality (as shown in Fig. 6). For nonlinear controller parameter tuning, the design steps mentioned in Section III can be used. As for the traditional proportional-integral (PI) controller, the parameter tuning procedure is based on the principle of loop-shaping mentioned in [14].

C. Time-varying voltage reference: resistive load

The first experiment consider the DC/DC boost converter connected to a constant resistive load of 12Ω , with goal

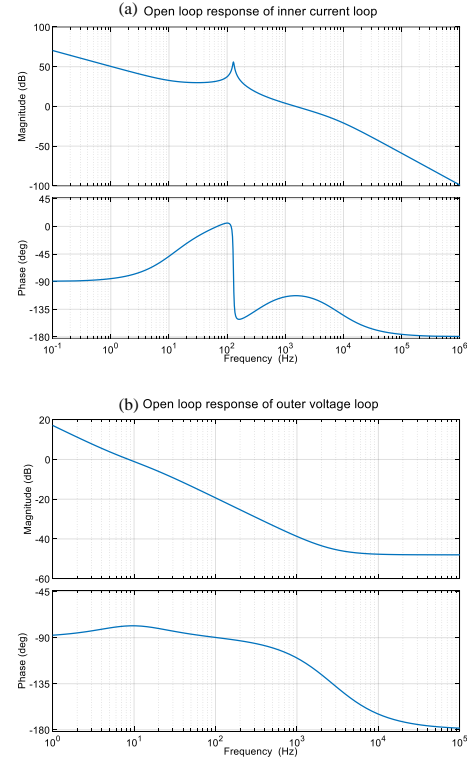


Fig. 4. The Bode diagram of the inner current loop and outer voltage loop.

to track a slowly time-varying output voltage reference. Fig. 5 shows how both the PI and the suggested NL controller perform well in tracking the desired reference profile for the output voltage dynamics.

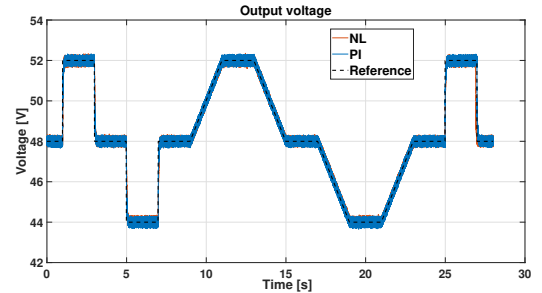


Fig. 5. Time-varying voltage reference: resistive load; The tracking of the output voltage reference.

Fig. 6 better remarks how both controllers have almost the same dynamics for the voltage. This is due to the chosen control gains, which are tuned to the goal to provide a fair comparison between the two controllers. For PI controller, the time constant is around 15 ms , while for the NL controller it is approximately 25 ms ; however, both controllers have a similar 95% settling time (around 100 ms) thus showing a similar behaviour. However, the PI controller causes less oscillations in the current in the inductance, as shown in Fig. 7. We stress that we used this experiment to tune the control gains such to obtain a comparable behaviour among the two controllers in terms of convergence rate and settling

time. In fact, the ratio for the PI voltage control parameters $\frac{K_p}{K_i} = \frac{0.3}{15} = 0.02$, and the ratio for the NL voltage control parameter $\frac{K_2^\xi}{K_1^\xi} = \frac{400}{15000} = 0.0266$ are sufficiently close to have similar behaviour. Similarly, the ratio between the proportional term for the PI and the error term for the NL, i.e., $\frac{K_p}{K_2^\xi}$, is in the order of magnitude of the capacitor C . The same reasoning can be applied for the integral term for the PI and the integral error term for the NL: $\frac{K_i}{K_1^\xi}$.

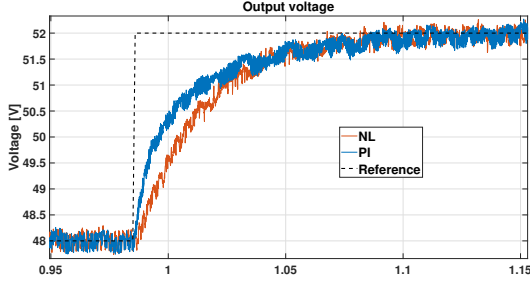


Fig. 6. Time-varying voltage reference: resistive load; Zoon of Fig. 5.

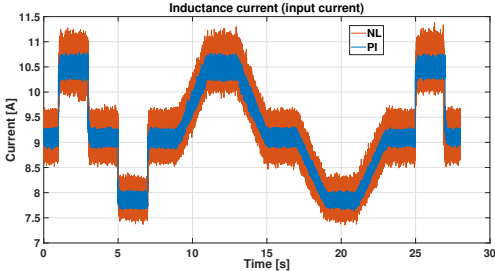


Fig. 7. Time-varying voltage reference: resistive load; The inductance current.

D. Constant voltage reference with resistive load variation

In the second experiment, the reference for the output voltage is constant at 48 V and, contrarily to the first situation, loads perturbations are included now. The considered load sequence is as follows: between $0 \leq t < 0.5$, the load is 12 Ω ; between $0.5 \leq t < 1.5$, the load is 8.57 Ω ; between $1.5 \leq t < 2.5$, the load is 6.66 Ω ; between $2.5 \leq t < 3.5$, the load is 8.57 Ω ; between $3.5 \leq t \leq 4$, the load is again 12 Ω .

Fig. 8 shows the output voltage, i.e., the load voltage. It is noticed that both controllers succeed in keeping the desired voltage reference, but the NL controller has a shorter transient and a smaller overshoot at each load change. This can be better appreciated in the zoom in Fig. 9, which considers the load variation taking place around 0.5s from 12 Ω to 8.57 Ω . Indeed, when using the PI controller the voltage reaches a minimum level of 44 V (8.3% with respect to the nominal value), while with the NL controller only a value of 46.5 V (3.1% with respect to the nominal value). Also, it takes 220 ms to come back to the nominal value with the PI, while only 80 ms with the suggested NL controller.

Fig. 10 shows the inductance current. Similarly to the time-varying voltage reference case in Section IV-C, the ripple is of minor magnitude when considering the PI controller with

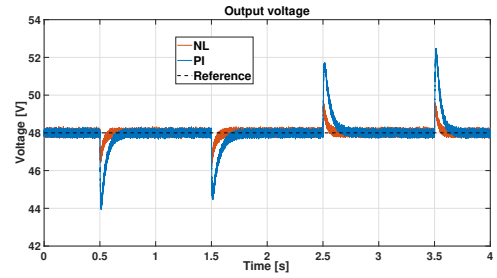


Fig. 8. Constant voltage reference with resistive load variation; The output voltage.

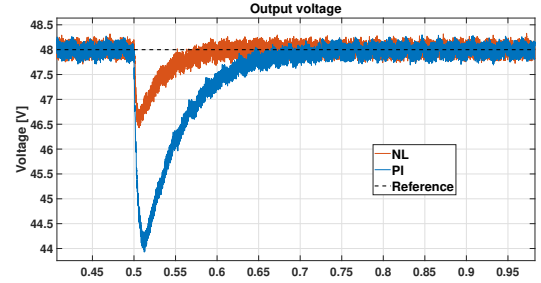


Fig. 9. Constant voltage reference with resistive load variation; Zoom of Fig. 8.

respect to the NL one. However, in this case we clearly remark a shorter transient when using the NL controller, as expected since Fig. 8 and 9.

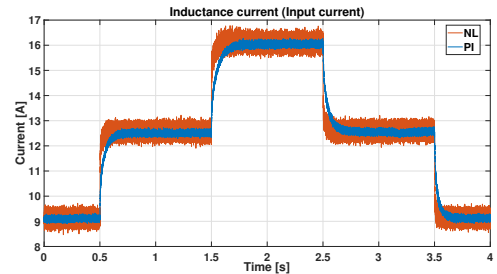


Fig. 10. Constant voltage reference with resistive load variation; The inductance current.

Finally, Fig. 11 shows the load voltage with respect to the load current. We remark on how the range of operation is slower with the NL controller (or, in other words, there are less variations with respect to the voltage reference). The slope of the lines is the resistance of the load, and clearly it is different depending on the load.

E. Time-varying voltage reference: CPL

Similarly to the experiment in Section IV-C, we consider here the goal to track a slowly time-varying output voltage reference, but the DC/DC boost converter is now connected to a CPL of 200 W. Fig. 12 shows the desired output voltage reference, i.e., the load voltage, and how both the PI and the NL controller successfully perform the tracking, as both controllers have a similar settling time. However, the NL controller produces no overshoot, as it is possible to appreciate also in the zoom in Fig. 13. In the selected time window, there

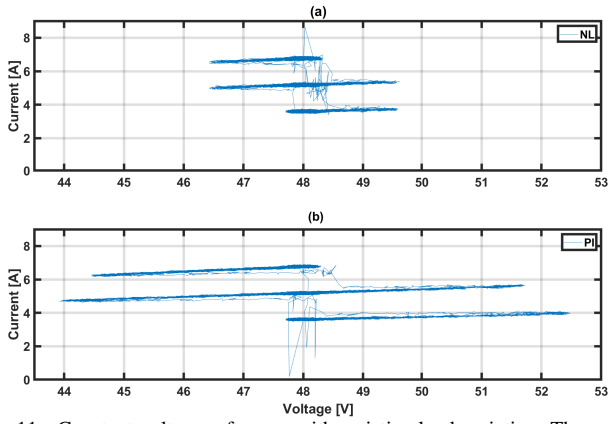


Fig. 11. Constant voltage reference with resistive load variation; The output voltage VS the output current. (a) NL; (b) PI.

is a peak of 53.2 V (2.5% with respect of nominal value) that does not take place with the NL. Both have a similar settling time of around 100 ms .

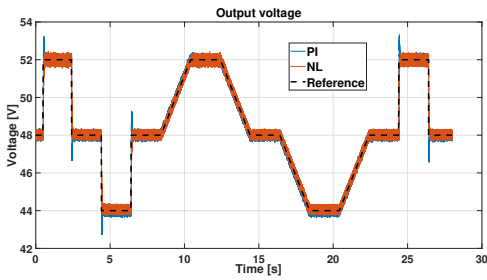


Fig. 12. Time-varying voltage reference: CPL; The output voltage.

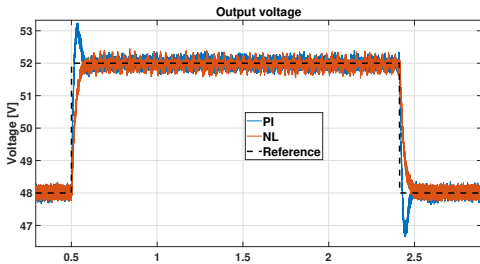


Fig. 13. Time-varying voltage reference: CPL; A zoom of the output voltage.

Fig. 14 shows how the inductance current is almost constant during the whole considered time window, no matter how the voltage varies. This is consistent with the CPL behaviour. Similarly to the previous cases in Sections IV-C and IV-D, the NL controller produces a higher ripple. Fig. 14 represents a zoom of Fig. 14, and shows more in detail how the NL controller does not produce any overshoot.

Finally, Fig. 16 presents the load current with respect to the load voltage. We remark on how the operating points follow an hyperbola as it should be.

F. Constant voltage reference with different CPLs

Let us now consider the goal to track a constant voltage reference of 48 V in case of several values for the CPL

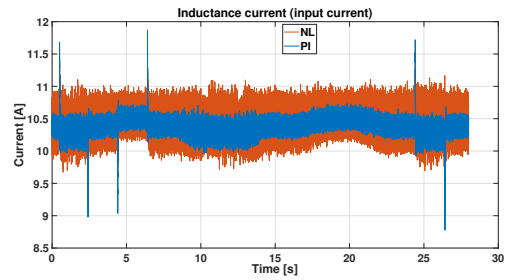


Fig. 14. Time-varying voltage reference: CPL; The inductance current.

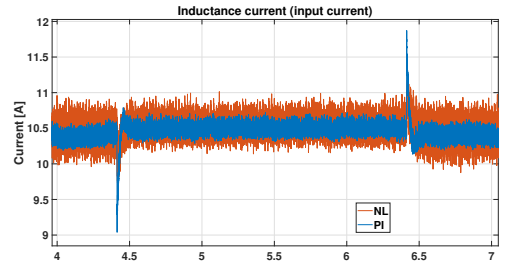


Fig. 15. Time-varying voltage reference: CPL; A zoom of the inductance current.

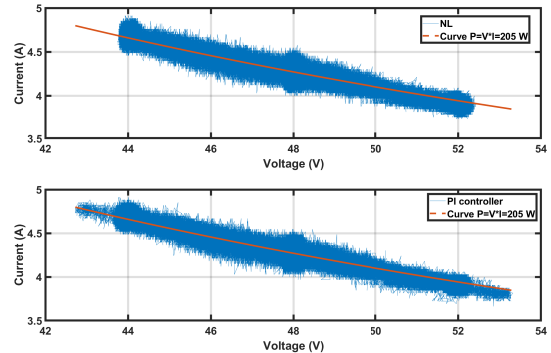


Fig. 16. Time-varying voltage reference: CPL; The output voltage VS the output current. (a) NL; (b) PI. The red line describes the power at 205 [W]

(100, 200, 300 and 400 W . Fig. 17 shows how both the PI and NL controllers successfully counteract to the CPL variation. However, as also noticed in the zoom-in Fig. 18, we remark that the settling time is shorter when using the NL with respect to the PI, and there are also smaller overshoots. More in detail, in the considered time window in Fig. 18 around 2.5 s , the PI produces a higher peak of 24 % with respect to nominal value instead of the one of 6 % with the NL and has a higher settling time of 200 ms compared to the one of 100 ms for the NL.

Fig. 19 shows the inductance current. Differently from the previous cases, the ripple is comparable between the PI and the NL controllers. Moreover, as a consequence of the advantages of the NL with respect to the PI shown in Fig. 17 and 18, we remark that the settling time is shorter and the overshoot is of minor magnitude when using the NL controller.

Fig. 20 shows the load current with respect to the load voltage. It is possible to see how the region in the plane follows a different hyperbola depending of the load value. Also, we remark that the operating region is smaller in case of NL

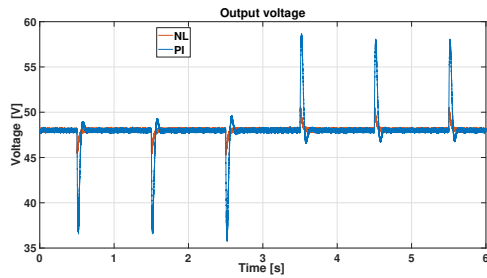


Fig. 17. Output voltage waveform at constant reference under different power of CPL.

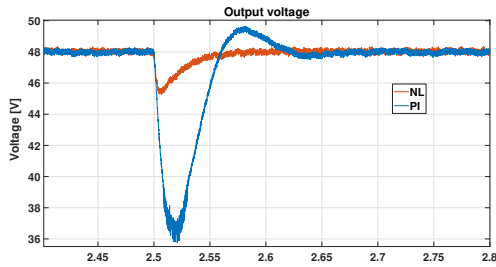


Fig. 18. Zoom of output voltage waveform at constant reference under different power of CPL shown in Fig. 17.

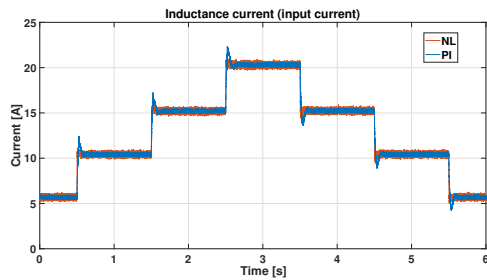


Fig. 19. Inductance current waveform at constant reference under different power of CPL.

controller, thus showing a more performing behaviour with respect to the PI one.

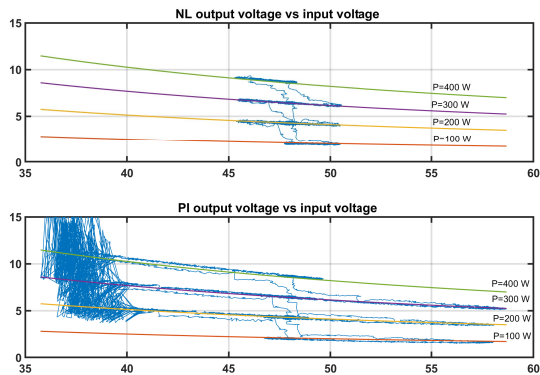


Fig. 20. Load voltage VS load current waveforms at constant reference under different power of CPL.

In Fig. 21a the error between the load voltage and the reference is shown. In Fig. 21b the phase plane for the error and the derivative of the error is provided. It is possible to

remark that the NL controller has much better performance than the PI one.

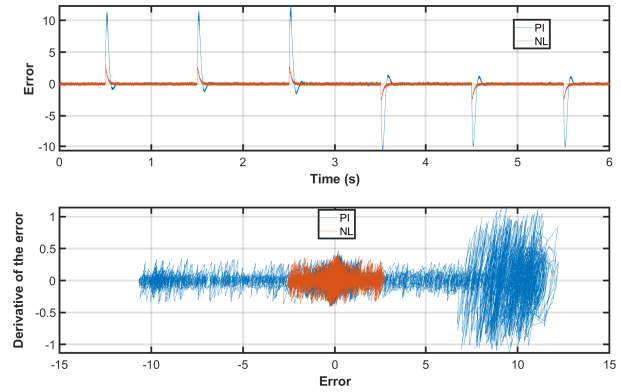


Fig. 21. Phase plane for error VS derivative of the error at constant reference under different power of CPL.

Table II summarizes the main characteristics of the PI controller and the suggested NL one. The comparison is both quantitative and qualitative. The performance evaluation indicators are classified into three groups: reliability and safety, electromagnetic pollution, and implementation challenges. While the NL strategy does not show notable enhancements over the classic PI controller when the boost converter feeds a resistive load, it considerably outperforms the PI when the converter supplies a CPL. For example, the voltage drop after load variation is significantly reduced to 6% of the nominal voltage, compared to a drop of 24% for the PI controller. Besides, the NL controller exhibits no voltage overshoot for step-up voltage tracking in case of CPL.

TABLE II
GLOBAL COMPARISON BETWEEN PI AND NONLINEAR CONTROL¹

Methods	PI	NL
Reliability and safety		
Voltage tracking 95% settling time with resistive load (Fig. 6)	≈100ms	≈100ms
Voltage drop after resistive load variation (Fig. 8)	8.3%	3.1%✓
Settling time after resistive load variation (Fig. 9)	220ms	80ms✓
Voltage drop after constant power load variation (Fig. 18)	24%	6% ✓
Settling time after constant power load variation (Fig. 18)	200ms	100ms✓
Voltage tracking with constant power load (Fig. 13)	an overshoot of 2.5% nominal voltage	no overshoot ✓
Number of sensors	2	2
Electromagnetic pollution		
Switching frequency	20kHz constant	20kHz constant
Implementation challenge		
Complexity of practical implementation	low	low

¹Check marks ✓ highlight the best performance for each criterion.

V. CONCLUSIONS

A nonlinear controller based on singular perturbation and dynamic feedback linearization is suggested in the present

paper for DC/DC boost converters, and its validation is performed in four experiments considering resistive loads and CPLs. Both the theoretical stability analysis and the experimental validation ensure that the proposed nonlinear controller provides performance and adaptability to a wide range of operating conditions with respect to classical linear control techniques. Moreover, the paper provides a detailed and implementation-oriented description of the controller for an easier understanding of the theoretical principles at its foundation and an intuitive tuning of the control parameters.

Future works will focus on adaptive approaches for uncertain parameters of the DC/DC converter and on numerically compute the optimal tuning of the control parameters to obtain the largest stability region with respect to desired performance. Moreover, the experimental validation of the proposed nonlinear controller when stabilizing a DC Microgrid is of interest.

REFERENCES

- [1] R. W. Erickson and D. Maksimovic, *Fundamentals of Power Electronics*. Springer, 2001.
- [2] D. Kumar, F. Zare, and A. Ghosh, "Dc microgrid technology: System architectures, ac grid interfaces, grounding schemes, power quality, communication networks, applications, and standardizations aspects," *IEEE Access*, vol. 5, pp. 12230–12256, 2017.
- [3] T. Dragičević, S. Vazquez, and P. Wheeler, "Advanced control methods for power converters in dg systems and microgrids," *IEEE Transactions on Industrial Electronics*, vol. 68, no. 7, pp. 5847–5862, 2021.
- [4] G. Escobar, R. Ortega, H. Sira-Ramirez, J.-P. Vilain, and I. Zein, "An experimental comparison of several nonlinear controllers for power converters," *IEEE Control Systems Magazine*, vol. 19, no. 1, 1999.
- [5] I. H. Kim and Y. I. Son, "Regulation of a dc/dc boost converter under parametric uncertainty and input voltage variation using nested reduced-order pi observers," *IEEE Transactions on Industrial Electronics*, vol. 64, no. 1, pp. 552–562, 2017.
- [6] E. Song, A. F. Lynch, and V. Dinavahi, "Experimental validation of nonlinear control for a voltage source converter," *IEEE Transactions on Control Systems Technology*, vol. 17, no. 5, pp. 1135–1144, 2009.
- [7] J. C. Mayo-Maldonado, O. F. Ruiz-Martinez, G. Escobar, J. E. Valdez-Resendiz, T. M. Maupong, and J. C. Rosas-Caro, "Nonlinear stabilizing control design for dc–dc converters using lifted models," *IEEE Transactions on Industrial Electronics*, vol. 68, no. 11, pp. 10772–10783, 2021.
- [8] R. Errouissi, A. Al-Durra, S. Muyeen, and A. El Aroudi, "Robust feedback-linearisation control of a boost converter feeding a grid-tied inverter for pv applications," *IET Power Electronics*, vol. 11, no. 3, pp. 557–565, 2018.
- [9] F. P. Priya and K. Latha, "Feedback linearization control of boost converter," in *2019 2nd International Conference on Intelligent Computing, Instrumentation and Control Technologies (ICICICT)*, vol. 1, 2019.
- [10] R.-J. Wai and L.-C. Shih, "Design of voltage tracking control for dc–dc boost converter via total sliding-mode technique," *IEEE Transactions on Industrial Electronics*, vol. 58, no. 6, pp. 2502–2511, 2011.
- [11] S.-C. Tan, Y. M. Lai, C. K. Tse, L. Martínez-Salamero, and C.-K. Wu, "A fast-response sliding-mode controller for boost-type converters with a wide range of operating conditions," *IEEE Transactions on Industrial Electronics*, vol. 54, no. 6, pp. 3276–3286, 2007.
- [12] P. Karamanakos, T. Geyer, and S. Manias, "Direct Voltage Control of DC–DC Boost Converters Using Enumeration-Based Model Predictive Control," *IEEE Transactions on Power Electronics*, vol. 29, no. 2, pp. 968–978, 2014.
- [13] A. Sferlazza, C. Albea-Sanchez, L. Martínez-Salamero, G. García, and C. Alonso, "Min-type control strategy of a dc–dc synchronous boost converter," *IEEE Transactions on Industrial Electronics*, vol. 67, no. 4, pp. 3167–3179, 2020.
- [14] Q. Guo, I. Bahri, D. Diallo, and E. Berthelot, "Model predictive control and linear control of dc–dc boost converter in low voltage dc microgrid: An experimental comparative study," *Control Engineering Practice*, vol. 131, p. 105387, 2023.
- [15] Y. Li, S. Sahoo, T. Dragičević, Y. Zhang, and F. Blaabjerg, "Stability oriented design of model predictive control for dc/dc boost converter," *IEEE Transactions on Industrial Electronics*, pp. 1–10, 2023.
- [16] J. W. Kimball and P. T. Krein, "Singular perturbation theory for dc–dc converters and application to pfc converters," *IEEE Transactions on Power Electronics*, vol. 23, no. 6, pp. 2970–2981, 2008.
- [17] H. Li, Z. Zhang, and Q. Liu, "Multi-time scale stability analysis of two-stage boost inverter based on floquet theory and harmonic balance method," in *2022 IEEE 31st International Symposium on Industrial Electronics (ISIE)*, pp. 843–850, 2022.
- [18] T. A. F. Theunisse, J. Chai, R. G. Sanfelice, and W. P. M. H. Heemels, "Robust global stabilization of the dc–dc boost converter via hybrid control," *IEEE Transactions on Circuits and Systems I: Regular Papers*, vol. 62, no. 4, pp. 1052–1061, 2015.
- [19] A.-C. Braitor, G. C. Konstantopoulos, and V. Kadiramanathan, "Current-limiting droop control design and stability analysis for parallel boost converters in dc microgrids," *IEEE Transactions on Control Systems Technology*, vol. 29, no. 1, pp. 385–394, 2021.
- [20] H. Sira-Ramirez and R. Silva-Ortigoza, *Control Design Techniques in Power Electronics Devices*. Springer, 2006.
- [21] A. Isidori, *Nonlinear control systems: an introduction*. Springer, 1985.
- [22] H. K. Khalil, *Nonlinear control*, vol. 406. Pearson New York, 2015.
- [23] E. Garza-Arias, J. C. Mayo-Maldonado, J. E. Valdez-Resendiz, G. Escobar, J. C. Rosas-Caro, and D. Guillen, "Direct output-voltage control of nonminimum phase higher order dc–dc converters," *IEEE Transactions on Industrial Electronics*, vol. 70, no. 2, pp. 1455–1466, 2023.
- [24] A. Isidori, "The zero dynamics of a nonlinear system: From the origin to the latest progresses of a long successful story," *European Journal of Control*, vol. 19, no. 5, pp. 369–378, 2013.
- [25] D. Zonetti, R. Ortega, and A. Benchaib, "Modeling and control of hvdc transmission systems from theory to practice and back," *Control Engineering Practice*, vol. 45, pp. 133–146, 2015.
- [26] P. Kokotović, H. K. Khalil, and J. O'reilly, *Singular perturbation methods in control: analysis and design*. SIAM, 1999.
- [27] P. Rouchon, "Necessary condition and genericity of dynamic feedback linearization," *J. Math. Systems Estim. Control*, vol. 4, no. 2, pp. 257–260, 1994.
- [28] Y. Chen, M. Jiménez Carrizosa, G. Damm, F. Lamnabhi-Lagarrigue, M. Li, and Y. Li, "Control-induced time-scale separation for multiterminal high-voltage direct current systems using droop control," *IEEE Transactions on Control Systems Technology*, vol. 28, no. 3, 2020.
- [29] J. Hauser, S. Sastry, and G. Meyer, "Nonlinear control design for slightly non-minimum phase systems: Application to V/STOL aircraft," *Automatica*, vol. 28, no. 4, pp. 665–679, 1992.
- [30] F. Perez, A. Iovine, G. Damm, and P. Ribeiro, "DC microgrid voltage stability by dynamic feedback linearization," in *2018 IEEE International Conference on Industrial Technology (ICIT)*, pp. 129–134, 2018.
- [31] A. Iovine, M. Jiménez Carrizosa, E. De Santis, M. D. Di Benedetto, P. Pepe, and A. Sangiovanni-Vincentelli, "Voltage regulation and current sharing in dc microgrids with different information scenarios," *IEEE Transactions on Control Systems Technology*, vol. 30, no. 5, 2022.
- [32] A. Jusoh, "The instability effect of constant power loads," in *PECon 2004. Proceedings. National Power and Energy Conference, 2004.*, pp. 175–179, 2004.
- [33] E. Hossain, R. Perez, A. Nasiri, and S. Padmanaban, "A comprehensive review on constant power loads compensation techniques," *IEEE Access*, vol. 6, pp. 33285–33305, 2018.
- [34] M. Cespedes, L. Xing, and J. Sun, "Constant-power load system stabilization by passive damping," *IEEE Transactions on Power Electronics*, vol. 26, no. 7, pp. 1832–1836, 2011.



Qihao Guo was born in Xinyang, China. He received the B.S. and M.S. degrees in electrical engineering from Beijing Jiaotong University, Beijing, China, in 2017 and 2020, respectively. He also obtained the general engineering degree from Ecole Centrale de Lille, Villeneuve d'Ascq, France. He is preparing the Ph.D. degree in the Group of Electrical Engineering of Paris (GeePs), Gif-Sur-Yvette, France. His research interests include modelling and control of electrical machines, control of DC-DC converter, and stability analysis of DC microgrid.



Miguel Jiménez Carrizosa received the M.S. Industrial Engineering degree in electrical engineering from the Universidad Politécnica de Madrid (UPM), Madrid, Spain, in 2011, the M.S. degree in energy systems from Supélec, Gif-sur-Yvette, France, in 2011, and the Ph.D. degree in electrical engineering and automatic control from Paris-Sud XI University, Orsay, France, in 2015. He is currently an Assistant Professor with the "Departamento de Energía y Combustibles", Escuela Técnica Superior de Ingenieros de Minas y Energía, UPM, and researcher

with the Centro de Electrónica Industrial (CEI-UPM). His research interests include HVDC systems, control of power converters, transmission and distribution systems, integration of renewable energies, smart grids, and optimal power flow methods.



Alessio Iovine (M'18) received the B.Sc. and M.Sc. degrees in electrical engineering and computer science from the University of L'Aquila, L'Aquila, Italy, in 2010 and 2012, respectively, and the European Doctorate degree in information science and engineering in 2016 from the University of L'Aquila, L'Aquila, Italy, in collaboration with CentraleSupélec, Paris-Saclay University, Paris, France. From 2016 to 2020, he held Post-Doctoral positions at University of L'Aquila, Efficacity Research Center (France), University of California at Berkeley

(USA), and CentraleSupélec. Currently, he is a Researcher at CNRS and a member of L2S, Paris-Saclay University. His research interests are related on advanced control methods for power and energy systems and traffic control, with smartgrids, integration of renewables and storage devices, autonomous vehicles and cooperative intelligent transportation systems as core applications.



Amir Arzandé received the M.S. and Ph.D. degrees in electrical engineering from "Pierre et Marie Curie" University, Paris, France, in 1980 and 1984, respectively. Since then, he has been a Full-Time Professor with the University of Supélec (École Supérieure d'Électricité), Paris, France. His research interests include digital control of electrical machines, power electronics for aerospace applications, and renewable energy integration to the grid